# Maneuver Optimization for Synthetic Aperture based DOA estimation of GNSS Jammers

Gerald LaMountain and Pau Closas
*Department of Electrical and Computer Engineering*
*Northeastern University*
Boston, MA

***Abstract*—GNSS denial via jamming is a low skilled attack which can be performed by nearly anyone using tools which are readily available through the online marketplace. Methods of jammer mitigation such as beamforming or other active methodologies require an estimation of the location of the jamming signal source. There is interest in developing systems which can be used to identify and locate the sources of broadcast signals, either for the purposes of augmenting mitigation or for the purposes of taking direct action to eliminate the sources of jamming signals. One way that such localization systems might be deployed is on rotor-wing aircraft which may be utilized to perform synthetic aperture direction of arrival (SA-DOA). In this contribution we propose a methodology for identifying circular maneuver trajectories which minimize the estimation error of performing SA-DOA using such a platform.**

***Index Terms*—Synthetic Aperture, Cramér-Rao Lower Bound, Bayesian Optimization, Pattern Search, Direction-of-Arrival**

## I. Introduction

As GNSS usage in PVT applications has become increasingly ubiquitous over the past several decades, denial or manipulation of GNSS signals has become an increasingly critical vulnerability in many civilian and military systems [1]–[3]. In particular, GNSS denial via jamming is a low skilled attack which can be performed by nearly anyone using tools which are readily available through the online marketplace. In order to combat these types of attacks on critical systems, substantial effort has been made into developing robust GNSS signal processing techniques. Some of these techniques have shown impressive results in mitigating the effect of jamming attacks, however there are no techniques capable of completely countering the loss of performance produced by jamming on GNSS based PVT [4], [5]. For this reason there is interest in developing systems which can be used to identify and locate the sources of broadcast signals, either for the purposes of augmenting mitigation techniques such as those which utilize beamforming or for the purposes of taking direct action to eliminate the sources of jamming signals. Passive jammer localization consists of two sages: first, the direction of arrival (DOA) of the jamming signal is estimated from several known locations, and second, the multiple direction of arrival estimates are used to compute an estimated location of the signal source. The final accuracy and precision of the location estimate depends on that of the direction of arrival estimates, and as such it is critical that the DOA estimates be as accurate and precise as possible.

For some applications it is not feasible or indeed desirable to have a fixed network of DOA estimators placed in established locations around a possible jamming source, for reasons which may be related to cost or mobility. For instance, antenna array receivers for GNSS are known to be complex to implement and bulky [6], although some solutions for the latter can be found in the literature [7]. In these instances, it may be necessary to perform DOA estimation based on alternative means; for instance, deployed on a mobile platform which can be relocated to different locations in the field in order to perform localization synthetically. The literature contains several examples of such systems deployed using unmanned aerial vehicles (UAV) equipped with small fixed sensor arrays consisting of two or three antennae or, on larger vehicles, rotating antenna arrays such as those utilized in airborne early warning and control (AEW&C) systems. Since jammer localization problems often occur on a scale which is not conducive to using large aircraft, many of these systems are restricted to small arrays which produce DOA estimates which are less precise, or more susceptible to error, in comparison to arrays consisting of larger numbers of antenna elements. In this contribution, we propose a broadcast source localization system which utilizes the advanced maneuvering capabilities of multi-rotor rotary-wing aircraft, including commercially available quadcopters, to perform a method of synthetic aperture direction of arrival (SA-DOA) estimation which may be able to produce more reliable estimates than comparable fixed-array (FA-DOA) estimation architectures deployed on similarly sized aircraft. In addition, we propose a methodology (see Fig. 1) in which present direction of arrival estimates may be used to optimize the parameters of the aircraft maneuvers used to perform SA-DOA in order to iteratively improve the achievable estimation accuracy based on the information inequality.

Implementation and testing of an architecture which accomplishes the above goals requires the completion of several intermediate steps, as detailed in Fig. 2. This paper discusses the derivation of a maximum likelihood estimator for DOA estimates based on a synthetic aperture antenna, for which we additionally provide its estimation bound provided by the Cramér-Rao Lower Bound (CRB). In the proposed architecture, the UAV performs an arbitrary trajectory (with known locations thanks to, for instance, an on-board inertial measurement unit) from which an initial DOA estimate can

978-1-7281-0244-3/20/$31.00 ©2020 IEEE


Authorized licensed use limited to: Northeastern University. Downloaded on May 24,2021 at 19:46:04 UTC from IEEE Xplore. Restrictions apply.

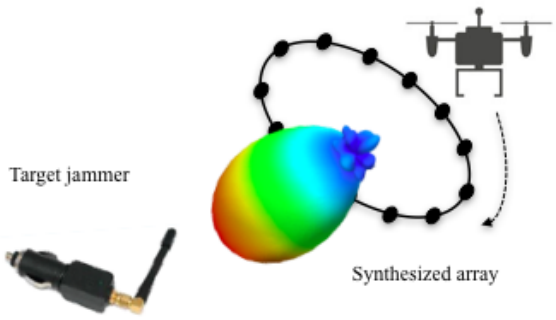


Fig. 1: Conceptual illustration of the proposed jamming localization technique. An UAV synthetizes array geometries in order to improve DOA estimation.

be performed. These initial estimate is required in order to evaluate the CRB and subsequently minimize it. To that aim, we consider two different optimization approaches to iteratively approach a solution.

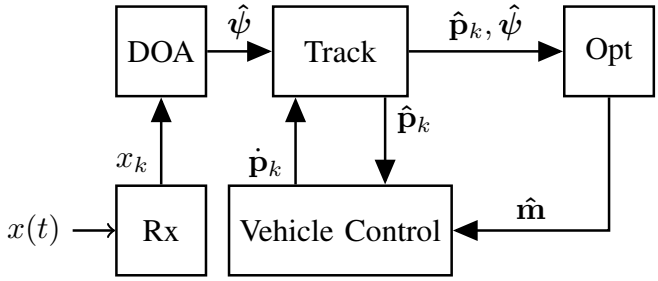


Fig. 2: Possible System Outline

The remainder of the paper is organized as follows. Section II introduces the signal model, derives the parameter estimation bounds, and formulates the maximum likelihood estimator for the problem. Section III discusses the maneuver optimization approach through minimization of the estimation bounds. Computer simulation results are discussed in Section IV and the paper is concluded with final remarks in Section V.

## II. Spatial filtering of RF signals with Synthetic Aperture Processing

### A. Signal Model for Synthetic Aperture Processing

The complex baseband representation of a line-of-sight (LOS) RF signal measured by a sensor is expressed as

$$x(t) = a(t)s(t - \tau(t))\exp(-j2\pi f_c \tau(t)) + n(t) \qquad (1)$$

Here, $s(t)$ is the baseband received signal content and $a(t)$ is the complex amplitude of the *received* signal produced when a signal of complex amplitude $u$ impinges on the antenna with directional gain and relative polarization $G(t) = F(t)\gamma(t)$. $\tau(t)$ is the delay caused by the propagation of the signal through space. $f_c$ is the nominal carrier frequency of the transmitted signal and $n(t)$ represents any additive noise, except from multipath reflections.

The delays observed in the received signal are separated into two components: the *reference* delay representing the propagation time for the transmitted signal to the origin of the local frame of reference of the receiver, and the *relative* delay representing the small differences in propagation time for different local antenna locations within that local frame of reference. That is,

$$\tau(t) = \tau_{\text{ref}} + \tau_{\text{rel}} \ . \qquad (2)$$

For small observation times and low relative velocities, the reference delay can be approximated to be of a constant value $\tau_{\text{ref}}(t) = \tau_0$, while the relative delay is expressed in terms of the position of the receiver in the local frame and a unit vector $\hat{\mathbf{r}}_\psi$ pointing in the direction of the transmitter as

$$\tau_{\text{rel}}(t) = \frac{\Delta\rho(t)}{c} = \frac{\hat{\mathbf{r}}_\psi^\top \mathbf{p}(t)}{c} \ . \qquad (3)$$

The relative delay, then, is consequently a function of the direction of arrival $\boldsymbol{\psi}$, comprised of the relative azimuth $\phi$ and elevation $\theta$ of the transmitter from the perspective of the receiver. When we collect a set of $K$ measurements of this signal at the receiver, we observe a measurement vector $\mathbf{x} \in \mathbb{C}^{K\times 1}$

$$\mathbf{x} = (\mathbf{d} \odot \mathbf{g})u + \mathbf{n} \ , \qquad (4)$$

where $\mathbf{d} \in \mathbb{C}^{K\times 1}$ is the basis-function vector with elements expressed in terms of the sample time $t_k$ as

$$[\mathbf{d}]_k = s(t - \tau(t_k))\exp(-j2\pi f_c \tau(t_k)) \ . \qquad (5)$$

$u \in \mathbb{C}^1$ is the complex constant amplitude of the signal impinging on the receiving antenna and $\mathbf{g} \in \mathbb{C}^{K\times 1}$ is the complex gain induced by the directionality and relative polarization of the antenna for each of the collected samples. For complex, real world radiation patterns this vector should be determined experimentally, but for some hypothetical cases however this may be computed analytically. In this paper we consider the case where each antenna is isotropic and right-hand circularly polarized (RHCP). Under these constraints, the value of $\mathbf{g}$ will depend only on the polarization mismatch coefficient $\gamma(t)$, which can be obtained as

$$\gamma(\mathbf{r}_\psi, \boldsymbol{\Upsilon}_{Rx}, \boldsymbol{\Upsilon}_{Tx}, \boldsymbol{\Gamma}_{Tx}, \boldsymbol{\Gamma}_{Rx}) = \boldsymbol{\phi}_{g,Tx}^H \boldsymbol{\phi}_{g,Rx} \ , \qquad (6)$$

where the vectors $\boldsymbol{\phi}_{g,Tx}$ and $\boldsymbol{\phi}_{g,Rx}$ represent the normalized Jones polarization vectors of the transmitting and receiving antennas transformed respectively into a global frame of reference. This transformation requires the application of two pairs of rotations. The first, $\boldsymbol{\Upsilon}_{Rx}, \boldsymbol{\Upsilon}_{Tx} \in \mathbb{R}^{3\times 3}$, are defined such that they each represent a transformation from the antenna's directional frame of reference (i.e. that in which the boresight of the antenna is aligned with the $z$ axis) into the global frame of reference. The second, $\boldsymbol{\Gamma}_{Rx}, \boldsymbol{\Gamma}_{Tx} \in \mathbb{R}^{3\times 3}$, are defined such that they each represent a transformation from the antenna's relative frame of reference (i.e. that in which the $z$ axis is aligned with $\mathbf{r}_\psi$ and $-\mathbf{r}_\psi$ respectively) into the global frame of



Authorized licensed use limited to: Northeastern University. Downloaded on May 24,2021 at 19:46:04 UTC from IEEE Xplore. Restrictions apply.

reference. Then, given the normalized Jones vector for RHCP, $\boldsymbol{\phi}_{RHCP} = 1/\sqrt{2}\left[1, -j, 0\right]^\top$, we can compute

$$\boldsymbol{\phi}_{g,Rx} = \boldsymbol{\Gamma}_{Rx}\boldsymbol{\Upsilon}_{Rx}\boldsymbol{\phi}_{RHCP} \tag{7}$$

$$\boldsymbol{\phi}_{g,Tx} = \boldsymbol{\Gamma}_{Tx}\boldsymbol{\Upsilon}_{Tx}\boldsymbol{\phi}_{RHCP} \tag{8}$$

### *B. Cramér-Rao Bound Derivation*

The Cramér-Rao Lower Bound (CRB) provides a lower bound on the covariance for joint, unbiased estimation of the deterministic parameters of a given model. The CRB is formed by taking the inverse of the Fisher information matrix (FIM) defined as

$$[\mathbf{J}(\boldsymbol{\xi})]_{ij} = -\mathbb{E}\left\{\frac{\partial^2 \ln p(\mathbf{x};\boldsymbol{\xi})}{\partial\xi_i \partial\xi_j}\right\} \tag{9}$$

where $\mathbf{x}$ is the vector of measurements and $\boldsymbol{\xi}$ is the vector of parameters to be estimated. Under the assumption that the measurement vector is distributed as $\mathbf{x} \sim \mathcal{CN}(\boldsymbol{\mu}(\boldsymbol{\xi}), \boldsymbol{\Sigma}_\mathbf{x})$, where $\boldsymbol{\Sigma}_\mathbf{x}$ does not depend on the parameters $\boldsymbol{\xi}$, application of the Slepian-Bang's formula yields

$$[\mathbf{J}(\boldsymbol{\xi})]_{ij} = 2\Re\left\{\frac{\partial\boldsymbol{\mu}^H(\boldsymbol{\xi})}{\partial\xi_i}\boldsymbol{\Sigma}_\mathbf{x}^{-1}\frac{\partial\boldsymbol{\mu}(\boldsymbol{\xi})}{\partial\xi_j}\right\} \tag{10}$$

For the model described in (4), we have

$$\boldsymbol{\mu}(\boldsymbol{\xi}) = (\mathbf{d}(\boldsymbol{v},\boldsymbol{\psi}) \odot \mathbf{g}(\boldsymbol{\psi}))u \tag{11}$$

with parameters

$$\boldsymbol{\xi} = \begin{bmatrix}\boldsymbol{u}\\ \boldsymbol{\psi}\\ \boldsymbol{\tau}_0\end{bmatrix}; \quad \boldsymbol{u} = \begin{bmatrix}\Re\{u\}\\ \Im\{u\}\end{bmatrix}; \quad \boldsymbol{\psi} = \begin{bmatrix}\theta\\ \phi\end{bmatrix}. \tag{12}$$

Under the assumption of a known channel spatio-temporal covariance matrix $\boldsymbol{\Sigma}_\mathbf{x}$, the FIM submatrices are given by [8], [9]

$$\mathbf{J}_{u_i u_j} = 2\Re\left\{\frac{\partial\boldsymbol{u}^H}{\partial u_i}(\mathbf{d}\odot\mathbf{g})^H\boldsymbol{\Sigma}_\mathbf{x}^{-1}(\mathbf{d}\odot\mathbf{g})\frac{\partial\boldsymbol{u}}{\partial u_j}\right\} \tag{13}$$

$$\mathbf{J}_{u_i \psi_j} = 2\Re\left\{\frac{\partial\boldsymbol{u}^H}{\partial u_i}(\mathbf{d}\odot\mathbf{g})^H\boldsymbol{\Sigma}_\mathbf{x}^{-1}\frac{\partial(\mathbf{d}\odot\mathbf{g})}{\partial\psi_j}\mathbf{u}\right\} \tag{14}$$

$$\mathbf{J}_{u_i \tau_0} = 2\Re\left\{\frac{\partial\boldsymbol{u}^H}{\partial u_i}(\mathbf{d}\odot\mathbf{g})^H\boldsymbol{\Sigma}_\mathbf{x}^{-1}(\frac{\partial\mathbf{d}}{\partial\tau_0}\odot\mathbf{g})\mathbf{u}\right\} \tag{15}$$

$$\mathbf{J}_{\psi_i \psi_j} = 2\Re\left\{\mathbf{u}\frac{\partial(\mathbf{d}\odot\mathbf{g})^H}{\partial\psi_i}\boldsymbol{\Sigma}_\mathbf{x}^{-1}\frac{\partial(\mathbf{d}\odot\mathbf{g})}{\partial\psi_j}\mathbf{u}\right\} \tag{16}$$

$$\mathbf{J}_{\psi_i \tau_0} = 2\Re\left\{\mathbf{u}\frac{\partial(\mathbf{d}\odot\mathbf{g})^H}{\partial\psi_i}\boldsymbol{\Sigma}_\mathbf{x}^{-1}(\frac{\partial\mathbf{d}}{\partial\tau_0}\odot\mathbf{g})\mathbf{u}\right\} \tag{17}$$

$$\mathbf{J}_{\tau_0 \tau_0} = 2\Re\left\{\mathbf{u}(\frac{\partial\mathbf{d}}{\partial\tau_0}\odot\mathbf{g})^H\boldsymbol{\Sigma}_\mathbf{x}^{-1}(\frac{\partial\mathbf{d}}{\partial\tau_0}\odot\mathbf{g})\mathbf{u}\right\} \tag{18}$$

The partial derivatives of $\mathbf{d}$ are separated as

$$\frac{\partial\mathbf{d}}{\partial\xi_i} = \frac{\partial\mathbf{d}}{\partial\boldsymbol{\tau}(t_k)}\frac{\partial\boldsymbol{\tau}(t_k)}{\partial\xi_i} \tag{19}$$

with

$$\begin{aligned}\left[\frac{\partial\mathbf{d}}{\partial\boldsymbol{\tau}(t_k)}\right]_k &= -\dot{s}(t_k - \tau(t_k)) \times \exp(j2\pi f_c\tau(t_k)))\\ &\quad - j2\pi f_c s(t_k - \tau(t_k))) \times \exp(j2\pi f_c\tau(t_k)))\end{aligned} \tag{20}$$

and

$$\left[\frac{\partial\boldsymbol{\tau}(t_k)}{\partial\xi_i}\right]_i = \begin{cases}1, & \text{if } \xi_i \in \boldsymbol{\tau}_0\\ c^{-1}\frac{\partial\Delta\rho(t_k)}{\partial\xi_i}, & \text{if } \xi_i \in \boldsymbol{\psi}\end{cases} \tag{21}$$

The values of $\partial\boldsymbol{u}/\partial\xi_i$ are $\begin{bmatrix}1, & 0\end{bmatrix}^\top$ for $\partial\boldsymbol{u}/\partial\Re\{u\}$ and $\begin{bmatrix}0, & j\end{bmatrix}^\top$ for $\partial\boldsymbol{u}/\partial\Im\{u\}$ respectively, with $j$ the unit imaginary operator. Finally, for $\mathbf{g}$ we need to compute the partial derivatives of the gain matrix with respect to the DOA parameters $\boldsymbol{\psi}$. These derivatives depend on the direction of arrival $\boldsymbol{\psi}$, as well as the radiation pattern and relative polarization of both the transmitting and receiving antennas. For the isotropic RHCP case, these derivatives can be computed analytically by applying the chain rule to (6) using the partial derivatives of the DOA vector

$$\frac{\partial\mathbf{r}_\psi}{\partial\theta} = \begin{bmatrix}-\sin\theta\cos\phi\\ -\sin\theta\sin\phi\\ \cos\theta\end{bmatrix}; \quad \frac{\partial\mathbf{r}_\psi}{\partial\phi} = \begin{bmatrix}-\cos\theta\sin\phi\\ \cos\theta\cos\phi\\ 0\end{bmatrix}; \tag{22}$$

### *C. Maximum-Likelihood Validation*

Under the assumption that the vector of received signal measurements is distributed as $\mathbf{x} \sim \mathcal{CN}(\boldsymbol{\mu}(\boldsymbol{\xi}), \boldsymbol{\Sigma}_\mathbf{x})$ with known spatio-temporal covariance matrix $\boldsymbol{\Sigma}_\mathbf{x}$, the probability of observing a given measurement vector $\mathbf{x}$ is given by the likelihood function

$$p(\mathbf{x};\boldsymbol{\xi}) = \frac{1}{\pi^n\det(\boldsymbol{\Sigma}_\mathbf{x}(\boldsymbol{\xi}))}\exp\left\{-(\mathbf{x}-\boldsymbol{\mu}(\boldsymbol{\xi}))^H\boldsymbol{\Sigma}_\mathbf{x}^{-1}(\mathbf{x}-\boldsymbol{\mu}(\boldsymbol{\xi}))\right\} \tag{23}$$

from which we define the maximum-likelihood solution for parameter vector $\boldsymbol{\xi}$ as

$$\hat{\boldsymbol{\xi}}_{\text{ML}} = \arg\max_{\boldsymbol{\xi}} p(\mathbf{x};\boldsymbol{\xi}) = \arg\max_{\boldsymbol{\xi}} \ln p(\mathbf{x};\boldsymbol{\xi}) \tag{24}$$

$$= \arg\min_{\boldsymbol{\xi}}(\mathbf{x}-\boldsymbol{\mu}(\boldsymbol{\xi}))^H\boldsymbol{\Sigma}_\mathbf{x}^{-1}(\mathbf{x}-\boldsymbol{\mu}(\boldsymbol{\xi})). \tag{25}$$

Here, $\ln p(\mathbf{x};\boldsymbol{\xi})$ is the log-likelihood function and the mean of the measurements is defined as in (4).

$$\boldsymbol{\mu}(\boldsymbol{\xi}) = \mathbb{E}\{\mathbf{x}\} = (\mathbf{d}\odot\mathbf{g})\mathbf{u} \tag{26}$$

Finding the maximum-likelihood estimate for the parameters $\hat{\boldsymbol{\xi}}$ is performed by solving an optimization problem with cost given by

$$\Lambda(\boldsymbol{\xi}) \triangleq (\mathbf{x}-\mathbf{h}\mathbf{u})^H\boldsymbol{\Sigma}_\mathbf{x}^{-1}(\mathbf{x}-\mathbf{h}\mathbf{u}) \tag{27}$$

where $\mathbf{h} \triangleq (\mathbf{d}\odot\mathbf{g})$. Since the mean function $\boldsymbol{\mu}(\boldsymbol{\xi})$ is linear with respect to the measurement amplitudes $\mathbf{u}$, we can formulate the maximum-likelihood solution for those parameters in closed-form as

$$\hat{\mathbf{u}}_{\text{ML}} = \left(\mathbf{h}^H\boldsymbol{\Sigma}_\mathbf{x}^{-1}\mathbf{h}\right)^{-1}\mathbf{h}^H\boldsymbol{\Sigma}_\mathbf{x}^{-1}\mathbf{x} \tag{28}$$

Substituting this back into (27) yields a new cost function in terms of the other parameters. Eliminating terms which are independent of the parameters $\boldsymbol{\xi}$ and simplifying yields the reduced cost function

$$[\Lambda(\boldsymbol{\xi})]_{\mathbf{u}=\hat{\mathbf{u}}_{\text{ML}}} = \mathbf{x}^H\boldsymbol{\Sigma}_\mathbf{x}^{-1}\mathbf{h}\left(\mathbf{h}^H\boldsymbol{\Sigma}_\mathbf{x}^{-1}\mathbf{h}\right)^{-1}\mathbf{h}^H\boldsymbol{\Sigma}_\mathbf{x}^{-1}\mathbf{x}\,, \tag{29}$$



Authorized licensed use limited to: Northeastern University. Downloaded on May 24,2021 at 19:46:04 UTC from IEEE Xplore. Restrictions apply.

to be maximized in this case. Recalling the definition of the basis function $\mathbf{d}$ given in (5), we see that, with respect to the parameters in $\boldsymbol{\psi}$ and $\boldsymbol{\tau}_0$, the cost function given in (29) is both nonlinear and nonconvex. Maximizing this function must be done numerically rather than analytically using a nonlinear optimization algorithm. Figure 3 shows the results of applying

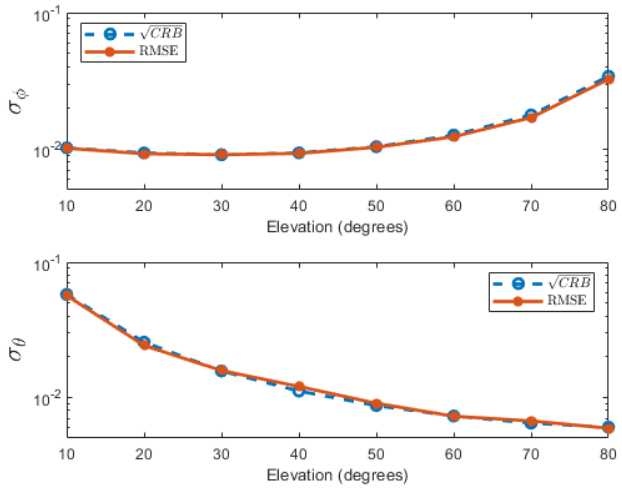


Fig. 3: RMSE for $50^\circ$ Azimuth, various Elevation angles (1000 Monte Carlo averages)

one such algorithm, the Nelder-Mead simplex method [10], to the cost function found in (5) for a known, uniform spatio-temporal covariance matrix of the form $\mathbf{\Sigma_x} = \sigma^2\mathbf{I}$. One-thousand trials were performed for different ground-truth directions of arrival and a noise variance of $\sigma = 10^{-1}$. The root mean squared error (RMSE) of these trials was computed and is shown in comparison to the results of the CRB computation described in II-B for a ground-truth azimuth of $50^\circ$ and varying elevation.

## III. Maneuver Optimization via CRB Minimization

We are interested in finding the set of sensor positions $\mathbf{p}(t)$ for a given observation interval $T_{SA}$ which will yield the best possible estimate of the parameters of interest in $\boldsymbol{\xi}$. To do this, we need to find the set of $k$ positions which minimize the Cramér-Rao lower bound defined in II-B. In particular, we are interested in minimizing the mean-squared error of our DOA estimate which can be done by minimizing the trace of the CRB submatrix corresponding to $\boldsymbol{\psi}$:

$$\hat{\mathbf{p}} = \underset{\mathbf{p}(t_k),\forall t_k \in T_{SA}}{\arg\min} \sum_i [\mathbf{J}(\boldsymbol{\xi})]^{-1}_{ii}, \forall \xi_i \in \boldsymbol{\psi} \tag{30}$$

With $\hat{\mathbf{p}} \in \mathbb{R}^{3\times k}$, estimating this set of positions is infeasible for even modest sample rates and observation intervals, and would yield a solution which would not be useful in controlling the sensor platform. Instead, we need to apply a more compact and tractable characterization of the position of the aircraft during the collection period.

### A. Maneuver Parameterization

To formulate our problem in a way that is independent of the sampling rate and observation interval, we need to identify a parameterization which yields a continuous function of position in terms of a handful of tunable design variables. This function defines a trajectory along which the sensor will travel during the observation interval. This can be done in a number of different ways, but in the case of synthetic aperture mounted on an aerial vehicle, it is appropriate to restrict ourselves to the set of circular trajectories incident to the current location of the vehicle. This yields the following characterization

$$\mathbf{p}(t) = f(t\,;\,\rho,\alpha,\beta,\gamma,\mathbf{p}_0,\mathbf{v}_0) \tag{31}$$

where $\rho$ is the radius of the maneuver, $\mathbf{p}_0$ and $\mathbf{v}_0$ are the initial position and velocity of the vehicle at the start of the maneuver, and $\alpha$, $\beta$, and $\gamma$ are the yaw, pitch and roll of the maneuver with respect to the initial position of the receiver, in the global frame of reference. By adjusting these parameters it is possible to form any complete or fractional circular trajectory incident to the current location of the receiver. Utilizing this parameterization for the position of the sensor into the formulation for the CRB given in II-B yields the following parameterization for the relative delay in (3) as a function of time

$$\tau_{\text{rel}}(t) = \frac{\hat{\mathbf{r}}_\psi^\top}{c} f(t\,;\,\rho,\alpha,\beta,\gamma,\mathbf{p}_0,\mathbf{v}_0) \tag{32}$$

Finally, this delay can be used to compute the value of $\mathbf{d}$ that is used throughout the CRB computation.

### B. Optimization Methods

The objective function to be minimized is the CRB described in II-B parameterized by the sample positions computed using (31). This nested complexity and lack of smoothness excludes the possibility of minimization using gradient-based optimization methods, so we must instead rely on *direct search methods* which require evaluating only the objective function at selected points. In our case, evaluating the objective function means computing the Cramér-Rao lower bound for a given set of trajectory parameters. To do so we must simulate the action of the sensor and signal for the entire duration of $T_{SA}$. Due to this computational cost, it is important that we minimize the number of evaluations required to reach a suitable global minimum. We consider two such methods for performing this direct search optimization: an algorithm based on generalized pattern searching (GPS) using an adaptive mesh [11], and Bayesian optimization method utilizing an expected improvement acquisition function [12].

*1) Generalized Pattern Search:* Generalized Pattern Search (GPS) describes a family of iterative algorithms for derivative-free unconstrained or linearly constrained optimization. These methods work by evaluating the objective function at a fixed set of points, called a mesh, which are located at a given distance in different directions away from the currently estimated minimum. This process is repeated for several iterations,



Authorized licensed use limited to: Northeastern University. Downloaded on May 24,2021 at 19:46:04 UTC from IEEE Xplore. Restrictions apply.

with the mesh distance being adjusted depending on whether or not the method was successful in identifying an improved minimum in the previous iteration. When an iteration identifies a new estimated minimum the mesh expands by a predetermined factor, otherwise it contracts. Application of linear constraints in the GPS algorithm is done by application of a barrier function of the form [13]

$$f_\Omega(\mathbf{x}) = \begin{cases} f(\mathbf{x}), & \text{if } \mathbf{x} \in \Omega \\ \infty, & \text{otherwise} \end{cases} \tag{33}$$

where $\Omega$ is the feasible set for $\mathbf{x}$. In this way, values which fall outside of the constraints are functionally discarded and the method proceeds with the remaining points in the mesh. The process of polling the objective function and updating the mesh repeats until a predetermined number of iterations have occurred, or the size of the mesh has reached a predetermined minimum. Although these methods can be applied to problems for which the objective function is non-differentiable or even non-continuous, they are not guaranteed to converge to a *global* minimum.

*2) Bayesian Optimization:* Bayesian optimization is another black box approach to globally optimizing objective functions, particularly those which are difficult or computationally expensive to evaluate or for which the objective function is not available in a closed form. It is similar to the pattern search algorithm in that it seeks to identify a global minimum in as few objective evaluations as possible, however the way in which it approaches this problem is fundamentally different. Rather than immediately searching the objective function for increasingly smaller values of the objective function, Bayesian optimization operates by constructing a probabilistic model over the feasible domain of the objective function. As observations are made by evaluating the objective function at different points, the posterior is updated and the model iteratively becomes a more refined representation of the true objective function [12].

Determining where to sample the objective function is done by invoking an acquisition function which quantifies the "utility" of a candidate point, taking into account the uncertainty in the probabilistic model and trading off between *exploration* and *exploitation*. Here, "exploration" refers to sampling the objective at points where the model uncertainty is high while, in the context of objective *minimization*, while "exploitation" refers to sampling the objective at points where the model expectation is low. By balancing these properties Bayesian optimization avoids becoming trapped in local minima, and in applications where it's useful can be exploited to find multiple local or global minima. For our application we selected the *expected improvement* acquisition function, which has the form

$$\mathrm{EI}(\mathbf{x}, Q) = \mathbb{E}[\max(0, \mu_Q(\mathbf{x}_{\text{best}}) - f(\mathbf{x})]. \tag{34}$$

where $f(x)$ is the objective function, $Q$ is the Gaussian process posterior, and $\mathbf{x}_{\text{best}}$ and $\mu_Q(\mathbf{x}_{\text{best}})$ are the location and value of its minimum. At each iteration the posterior distribution of the model is updated using samples of the objective function which correspond to the maximum of this function as computed in the previous step, and a new maximum is computed for the next iteration. This process is repeated for a fixed number of iterations corresponding to the total number of allotted objective function evaluations.

## IV. Experimental Validation

To compare the two methods for CRB optimization under the maneuver model described in III-A, we performed simulated experiments assuming known signal waveform $s(t)$ of a form consistent with a narrowband continuous-wave (CW) jammer modulated to a frequency appropriate for jamming GPS L1 (1575.42 MHz). Since the CRB for a uniform circular array is agnostic to relative azimuth, received signals were generated for an azimuth of $50^\circ$ above the xz-plane and elevations varied from $10^\circ - 90^\circ$ above the xy-plane in increments of $10^\circ$.

For each experiment, the initial direction-of-arrival was first computed using maximum likelihood estimation and an arbitrary trajectory with a radius of 2 meters in the xy-plane, executed at a vehicle speed of $2\pi$ m/s ($\pi$ rads/sec). This parameters given by this maximum likelihood result were then used to form the model for performing CRB optimization using both the pattern search and Bayesian optimization methods. Each method was initialized with the flat, arbitrary trajectory used to perform initial estimation and executed for a total of one-hundred function evaluations. After each iteration, the minimum objective and total number of function calls for each method was recorded. In the case of Bayesian optimization, additional random initialization points are selected each time the method is executed. In order to determine mean performance the method was called fifty times for each experiment and the results averaged.

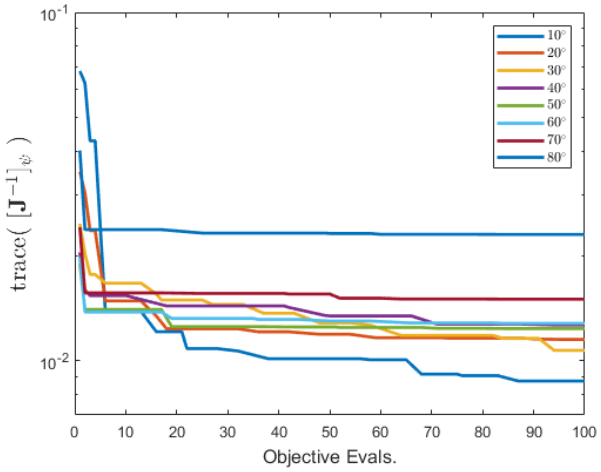


Fig. 4: DOA-Trace Objective function minimum using GPS optimization. Ground truth of $50^\circ$ Azimuth, various Elevation angles.

Figures 4 and 5 show the progression of estimated minima for the pattern search and Bayes algorithms respectively as a



Authorized licensed use limited to: Northeastern University. Downloaded on May 24,2021 at 19:46:04 UTC from IEEE Xplore. Restrictions apply.

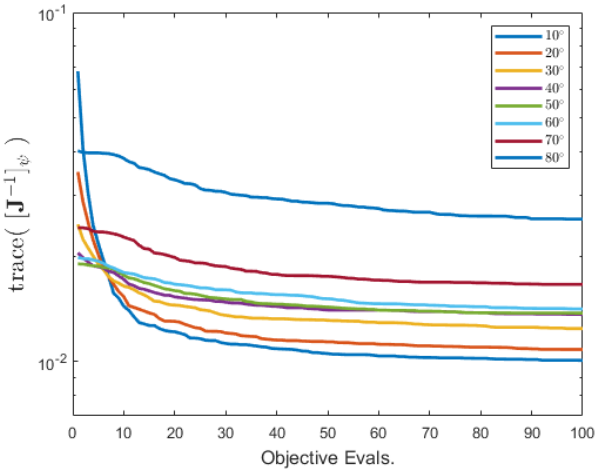


Fig. 5: DOA-Trace Objective function minimum using Bayesian optimization. Ground truth of $50^\circ$ Azimuth, various Elevation angles.

function the number of objective evaluations. Both methods were successful in identifying circular trajectories which perform better than the initial, flat trajectory. In comparison to each other the two methods performed similarly on average, with the GPS methods performing slightly better on average for evaluation counts lower than ten. This is consistent with the approach employed by each method: while the GPS methods are designed to rapidly converge on a local minimum, the Bayesian methods aim to strike a balance between searching for the minimum and mapping the function over the feasible domain.

## V. Conclusions

In this paper we have proposed a method for minimizing estimation error in unbiased estimators by finding tunable parameters which minimize the corresponding Cramér-Rao lower bound. We applied this method to the problem of direction-of-arrival (DOA) estimation in the context of GNSS jammer localization, and showed that this approach can be used to design trajectories for performing DOA estimation using an antenna mounted on rotor wing aircraft. Two different methodologies were applied to solving this minimization problem: one using generalized pattern search and another using Bayesian optimization with an expected improvement acquisition function. By applying these methods in simulations of the GNSS jammer localization scenario, we determined that both methods perform similarly for the given scenarios. We conclude that for the particular problem of optimizing DOA estimation in GNSS synthetic aperture, there is not a substantial benefit to applying more computationally complex Bayesian optimization methods where more efficient pattern search methods will suffice.

## Acknowledgment

This work has been partially supported by the NSF under Awards CNS-1815349 and ECCS-1845833.

## References

[1] Daniele Borio, Cillian O'Driscoll, and Joaquim Fortuny, "GNSS jammers: Effects and countermeasures," in *2012 6th ESA Workshop on Satellite Navigation Technologies (Navitec 2012) & European Workshop on GNSS Signals and Signal Processing*. IEEE, 2012, pp. 1–7.

[2] Daniele Borio, Fabio Dovis, Heidi Kuusniemi, and Letizia Lo Presti, "Impact and detection of GNSS jammers on consumer grade satellite navigation receivers," *Proceedings of the IEEE*, vol. 104, no. 6, pp. 1233–1245, 2016.

[3] Moeness G Amin, Pau Closas, Ali Broumandan, and John L Volakis, "Vulnerabilities, threats, and authentication in satellite-based navigation systems [scanning the issue]," *Proceedings of the IEEE*, vol. 104, no. 6, pp. 1169–1173, 2016.

[4] Daniel Medina, Christoph Lass, E Pérez-Marcos, Ralf Ziebold, Pau Closas, and J García, "On GNSS Jamming Threat from the Maritime Navigation Perspective," in *Proceedings of the 22st International Conference on Information Fusion (FUSION), Ottawa, ON, Canada*, 2019, pp. 2–5.

[5] Ruben Morales-Ferre, Philipp Richter, Emanuela Falletti, Alberto de la Fuente, and Elena Simona Lohan, "A survey on coping with intentional interference in satellite navigation for manned and unmanned aircraft," *IEEE Communications Surveys & Tutorials*, 2019.

[6] Carles Fernández-Prades, Javier Arribas, and Pau Closas, "Robust GNSS receivers by array signal processing: Theory and implementation," *Proceedings of the IEEE*, vol. 104, no. 6, pp. 1207–1220, 2016.

[7] John L Volakis, Andrew J O'Brien, and Chi-Chih Chen, "Small and adaptive antennas and arrays for GNSS applications," *Proceedings of the IEEE*, vol. 104, no. 6, pp. 1221–1232, 2016.

[8] Miguel Angel Ribot Sanfelix, *Parameter Estimation with GNSS-Reflectometry and GNSS Synthetic Aperture Techniques*, Ph.D. thesis, EPFL, Lausanne, 2018.

[9] Miguel Angel Ribot, Joaquin Cabeza, Pau Closas, Cyril Botteron, and Pierre-Andre Farine, "Estimation bounds for GNSS synthetic aperture techniques," in *2017 IEEE 7th International Workshop on Computational Advances in Multi-Sensor Adaptive Processing (CAMSAP)*. Dec. 2017, IEEE.

[10] John A Nelder and Roger Mead, "A simplex method for function minimization," *The computer journal*, vol. 7, no. 4, pp. 308–313, 1965.

[11] C. Bogani, M.G. Gasparo, and A. Papini, "Generalized pattern search methods for a class of nonsmooth optimization problems with structure," *Journal of Computational and Applied Mathematics*, vol. 229, no. 1, pp. 283 – 293, 2009.

[12] B. Shahriari, K. Swersky, Z. Wang, R. Adams, and N. De Freitas, "Taking the human out of the loop: A review of Bayesian optimization," *Proceedings of the IEEE*, vol. 104, no. 1, pp. 148–175, 2015.

[13] Charles Audet and J. E. Dennis, "Analysis of generalized pattern searches," *SIAM Journal on Optimization*, vol. 13, no. 3, pp. 889–903, Jan. 2002.



Authorized licensed use limited to: Northeastern University. Downloaded on May 24,2021 at 19:46:04 UTC from IEEE Xplore. Restrictions apply.